HiSST: 2nd International Conference on
High-Speed Vehicle Science & Technology
16–19 May 2022, Bruges, Belgium

Experimental Investigation of the Effect of Steps and Gaps on Hypersonic Vehicles

William Ivison[1], Chris Hambidge[2], Matthew McGilvray[3], Jim Merrifield[4], Johan Steelant[5]

Abstract

The design of hypersonic vehicles typically incorporates the use of simple, geometric shapes with smooth surfaces. There are many reasons why aircraft cannot have perfectly smooth surfaces with small, unavoidable imperfections frequently being present. These can appear in many forms, such as gaps between tiles and rivets joining different panels. Surface features like this are mainly detrimental to aircraft performance for two reasons: they can cause premature boundary layer transition, leading to higher integrated heat loads and unexpected aerodynamic loads; and they cause highly localised areas of heat flux augmentation – up to many times the undisturbed level. This work is part of a project which aims to characterise some of these effects using a combination of experimental and numerical techniques with the overall aim being to produce useful engineering level correlations for use in vehicle design. This paper presents initial experiments performed in the Oxford High Density Tunnel (HDT). Heat flux and pressure data have been acquired for a range of step and cavity geometries, and capability of a sophisticated experimental model has been shown.

Keywords: *heat flux, boundary layer transition, flat plate, step*

Nomenclature

Latin
c_p – Specific heat capacity at constant pressure
M – Mach number
p – Pressure
Pr – Prandtl number
q – Heat flux
Re – Reynolds number
St – Stanton number
T – Temperature
u – Velocity
Greek
γ – Ratio of specific heat capacities
ρ – Density
Subscripts
∞ – Freestream condition
0 – Stagnation condition
rec – Recovery condition
w – Wall condition

1. Introduction

Achieving sustained hypersonic flight poses many unique challenges which are not present at lower speeds. One of these challenges is the management of the high levels of heat flux experienced by the aircraft, this often forces designers to limit the Mach number [1]. Typically, to avoid additional generation of heat through hot spots incurred from steps, cavities, and gaps, high speed vehicles are designed with smooth bodies using simple geometric shapes. However, there are many reasons why in a practical vehicle it is unavoidable to maintain smooth external surfaces, including: allowance for thermal expansion between different components; actuation of control surfaces; inclusion of instrumentation; tolerance in manufacture and interfaces between different components; attachment points

[1] *Oxford Thermofluids Institute, University of Oxford, OX1 0ES, william.ivison@eng.ox.ac.uk*
[2] *Oxford Thermofluids Institute, University of Oxford, OX1 0ES, chris.hambidge@eng.ox.ac.uk*
[3] *Oxford Thermofluids Institute, University of Oxford, OX1 0ES, matthew.mcgilvray@eng.ox.ac.uk*
[4] *Fluid Gravity Engineering Ltd., Emsworth, Hampshire, PO10 7DX, jim.merrifield@fluidgravity.co.uk*
[5] *ESA-ESTEC, Keperlaan 1, 2200 AZ Noordwijk, Netherlands, johan.steelant@esa.int*

during launch and separation of stages; interfaces that are required for separation of deployable components. Hypersonic vehicle design is usually conservative with simple geometric aerodynamic shapes being preferred. However, gaps, interfaces and protuberances may be necessary due to the reasons outlined above. These surface imperfections can have a large impact on the nearby flow and can lead to various effects such as increased localised heating rates and premature boundary layer transition. Flows like this are difficult to analyse, meaning that any design process needs to carry high safety margins. Over-conservative design leads to excessive thermal protection, adding unnecessary weight, and suppressing aerodynamic performance. There is a need for engineering tools capable of simplifying the complex interactions between different components and quickly assessing the performance of vehicle designs to allow for quick changes between design iterations [2, 3]. Currently, only basic rules of thumb exists for sizing idealised gaps, interfaces, and protuberances such that they will not be significant in terms of aerothermodynamic effects. These are not capable of satisfying the need for useful engineering-level methods and tools. High quality correlations which can simply describe the effects of more representative surface imperfections at relevant flow conditions are necessary.

The aim of this work is to extend the current knowledge base to include more general correlations and rules of thumb which are more applicable to real hypersonic vehicle design. Extending the library of available databases and engineering level correlations will enable consideration of surface imperfections to be addressed more accurately in early design stages, ultimately leading to carrying less design margins in later phases. This will be achieved by combining experimental testing with numerical simulations. This paper presents an initial experimental campaign with the aim of proving the capability of a new experimental model which will be used in the future to collect data for a large range of surface geometries.

2. Test Facility

Testing took place in the Oxford High Density Tunnel (HDT). The HDT, a schematic of which is shown in Fig.1, features a 17.4 m long Ludwieg tube with internal diameter of 152 mm. The barrel of the Ludwieg tube forms a high pressure reservoir for the facility and is wrapped in external electrical heating to increase the total temperature of the test gas - up to 550 K. The barrel feeds a contoured converging/diverging nozzle via a fast-acting plug valve and a stagnation plenum. The nozzle has an exit diameter of approximately 350 mm and exhausts into a 760 mm diameter test section and then into a 28 m^3 vacuum tank external to the building. When the plug valve opens at the beginning of a shot the test gas expands through the nozzle, producing steady periods of cold hypersonic flow of 30 to 50 ms. More details on the construction and operation of the HDT can be found in references [4] and [5]. A freestream condition was chosen so that boundary layer transition was observed on the model after the inclusion of a step or protuberance. The initial fill pressure and temperature were set to meet desired freestream pressure and temperature. Details of this condition are listed in Table 1. The Reynolds number was calculated assuming isentropic expansion through the nozzle and viscosity was calculated using the Keyes relation [7].

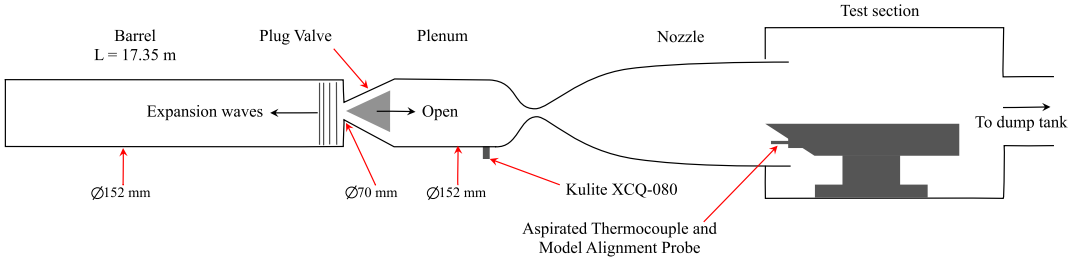

Fig 1. A schemtic of the Oxford High Density Tunnel (HDT), adapted from [6].

Table 1. Freestream condition for experiments

Mach Number	Re_{unit} million/m	p_0 bar	T_0 K
6	34.4	38.5	450

3. Test Model

For this work, a new highly configurable experimental model was developed. A flat plate model was used which incorporates two Thorlabs PIA25 piezoelectric inertia actuators, with 20 nm step size, to raise and lower blocks forming the upper surface of the model. The forward block is located 150 mm downstream of the leading edge and measures 5 mm in length and the rear block makes up the remainder of the flat plate: 392 mm in length. The model is 140 mm in width, with the actuated portion being 110 mm in width. The surface blocks can be moved with high repeatability and with a precision of order 0.01 mm. The height of each block was measured in real time using linear potentiometers internal to the model. Both blocks have a range of motion of ±4 mm and the total difference in height between the two parts of the geometry can be up to 8 mm.

The model was designed with the aim of being able to produce a wide variety of geometries to simulate different surface imperfections. These are summarised in Fig. 2: basic geometries being a flat plate, forward- and backward-facing steps, single 2D protuberances (referred to as steps in this paper), and cavities and gaps - these are indicated in the blue box. The model is also capable of producing combined geometries, the most realistic being stepped gaps, where the downstream edge of a gap is at a different height to the upstream edge. On a real vehicle this could be representative of a stepped tile in a tile array forming a thermal protection system (TPS) [8].

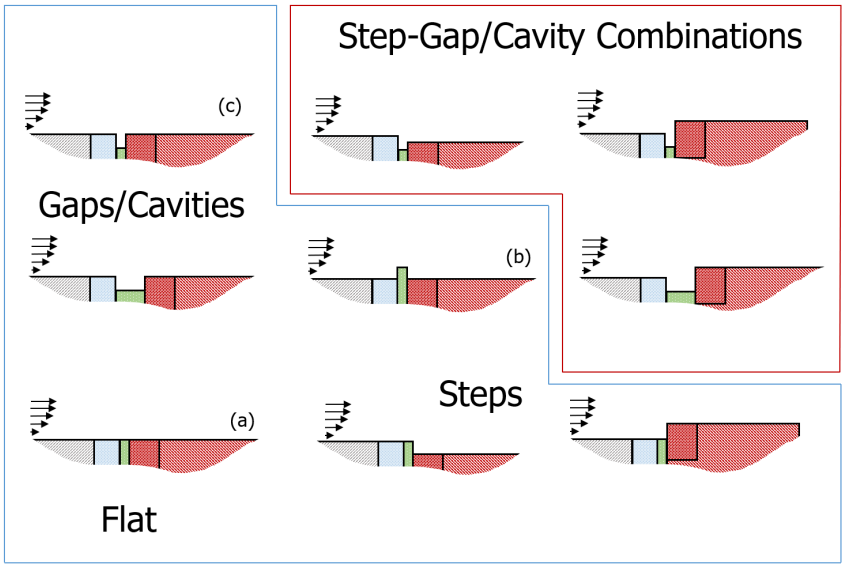

Fig 2. The range of surface geometries which the model can replicate.

During the initial testing presented in this paper, the rear block was kept at a constant height (0 mm) and only the forward block was actuated. This allowed three different geometry types to be tested: a flat plate, single 2D protuberances, and gaps/cavities. These geometries are marked (a), (b), and (c) in Fig. 2. Table 2 shows the sizes of the geometries which were tested. The boundary layer thickness at the step location was calculated to be 1.00 mm for the freestream condition tested.

During initial tests, the downstream instrumentation indicated high levels of turbulence in the boundary layer – this was confirmed by IR imaging to be caused by interference propagating downstream from

the leading edge. An extension piece was manufactured which effectively increased the width of the flat plate by 30 mm and moved the edge effects away from the gauges. The extension piece can be seen in Fig. 4.

Table 2. Range of geometries tested

Geometry		**Size** mm
Flat plate	(a)	-
Step	(b)	0.50
		0.75
		1.00
		1.28
Cavity	(c)	0.5
		1.00
		2.00

3.1. Instrumentation

A range of instrumentation was employed in order to investigate bouudnary layer properties and heat flux augmentation. A picture of the model with the locations of different instrumentation indicated is given in Fig.3.

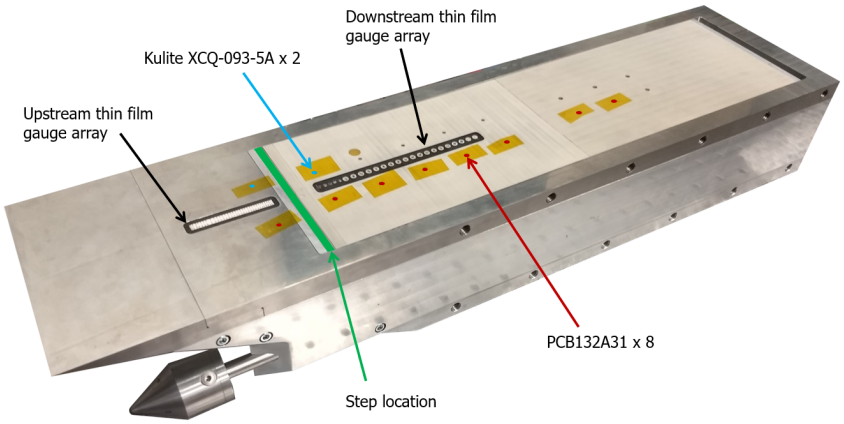

Fig 3. The experimental model with instrumentation indicated.

3.1.1. Heat flux gauges

Two arrays of thin film heat transfer gauges were used - one upstream of the step location (90 mm to 140 mm from the leading edge) containing 19 gauges and one downstream of the step location (170.5 mm to 287.5 mm from the leading edge) containing 11 gauges. Both arrays were located on the model centreline. The thin film gauges were manufactured in-house and were amplified using in-house HTA5 Lancaster amplifiers. Further details of the construction of the thin film gauges can be found in reference [9].

3.1.2. Surface pressure transducers

Eight PCB 132A31 high frequency pressure transducers were positioned 14.5 mm off-centreline. One of them was located upstream of the step location and the remaining seven were evenly spaced down-stream. These were amplified using PCB 483C05 ICP signal conditioners.

Additionally, two Kulite XCS-093-5A pressure transducers were used for steady state pressure measure-

ments. These were located off-centreline opposite the two most upstream PCB gauges. These were amplified using Fylde FE-H379-TA high speed transducer amplifiers.

3.1.3. Flow visualisation

A Telops Fast M3k Mid-Wave IR camera was mounted external to the tunnel to provide IR thermography.

3.1.4. Flow sensors

A model alignment probe was mounted to the front of the model underneath the leading edge. The probe consists of a cone with four Kulite XCEL-152-25A pressure transducers spaced equally around the conical face. By comparing the pressures on opposite sensors, the alignment of the model with the freestream can be verified.

An aspirated thermocouple was also mounted to a probe at the front of the model, consisting of an electrically heated thermocouple suspended across the front of a hollow cyclinder. This stagnates the flow and can provide a measurement of the freestream total temperature. Details of the construction and operation of aspirated thermocouples used in HDT can be found in reference [10].

4. Results

4.1. Heat Flux

Heat flux data was collected using thin film heat transfer gauges and an IR camera independently.

4.1.1. Thin Film Heat Transfer Gauges

Thin film heat flux gauges were used to evaluate overall heat flux during tests, the purpose of which being to assess the state of the boundary layer. Filtered voltage signals from the thin film gauges were converted to temperatures using Eq. 1 where values of α were pre-calibrated for each gauge. Gauge temperatures were then converted to surface heat fluxes using the impulse response method developed by Oldfield [11]. Heat fluxes were averaged over the test time and Stanton numbers were calculated according to Eq. 2, where the recovery temperature, T_{rec} was calculated using Eq. 3.

$$\Delta \mathrm{T} = V_{AC}\frac{1+\alpha T_1}{\alpha V_{DC}} \tag{1}$$

$$\mathrm{St} = \frac{q}{\rho_\infty u_\infty c_p (T_{rec} - T_w)} \tag{2}$$

$$T_{rec} = T_\infty (1 + \sqrt{\mathrm{Pr}_\infty}(\frac{\gamma - 1}{2})M_\infty^2) \tag{3}$$

Fig. 5a and Fig. 5b show the Stanton number distributions along the length of the model for steps and cavities, respectively. Also plotted are the van Driest and Eckert approximations for flat plate laminar and turbulent heating [12, 13]. The heat flux upstream of the step location follows the laminar flat plate correlations closely, indicating that the boundary layer upstream of the step is laminar in every test.

It can be seen that the presence of a step causes a decrease in heat flux upstream of the step, with the magnitude of this decrease increasing with larger steps. This effect is likely due to a thickening of the boundary layer upstream of the step which creates an area with a lower temperature gradient and a lower heat flux. A step of this height would be expected to produce a separation, which would increase local heat flux levels rather than decrease as seen in this data. However, due to the small step heights, the separation is thought to be happening much closer to the step where there is a gap in the instrumentation. This effect is also seen in references [14] and [15] where a significant decrease in surface heat flux is observed with small steps before the separation region causes a large increase. In this work, instrumentation is not located close enough to the step to see the effect of the separation region.

Downstream of the step, there is a consistent increase in heat flux. It is unclear whether this is due to reattachment of the boundary layer following a wake separation or the beginning of boundary layer transition. However, at step heights of 1 mm and 1.28 mm the heat flux approaches the predicted turbulent level.

Cavities appear to have no effect on heat flux compared to steps of similar sizes. There is no apparent difference between flat plate heat flux data and cavities of any size tested. Any differences are due to variation of tunnel conditions between shots.

In the heat flux data downstream of the step there is a large amount of scatter between adjacent gauges. This is most likely due to very slight differences in how the gauges were mounted into the plate. This theory is supported by the coherence of the scatter of different cavity depths in Fig. 5b. Some gauges were recessed and some protruded from the surface, whereas the gauges upstream of the step were painted onto a single piece of Macor. Although the differences in the heights of the gauges were small (<50 μm), the effect on heat flux is apparently significant. Additionally, flow disturbances originating from upstream gauges would have caused more scatter and uncertainty in downstream gauges (see IR thermography in Fig. 4).

4.1.2. IR Thermography

Limited IR thermography data was also collected – Fig. 4 shows IR data from two separate shots, with the same step height of 1 mm, overlaid on a CAD image of the model. Note that there is no scale for heat flux: the IR data collected during this work was only used as a qualitative tool for visualising the overall structure of the flow over the model. Various flow features can be seen: there is a distinct high heat flux area spreading from the lower side of the model. This is aligned with the interface between the leading edge and the main top plate (marked with a red cross) indicating a slight misalignment between these two plates. The extension piece added to the model (the additional area at the lower side of Fig. 4) is effective in moving this disturbance away from the model centreline. There are several instances of growth of turbulence, resulting in a fully turbulent boundary layer at the downstream end of the second image. The origin of these turbulent regions is unclear, but the instrumentation on the centreline of the model is likely to cause boundary layer disturbances which could grow into turbulence. Finally, there is a clear increase in heat flux towards the upstream edge of the step as well as decrease in the wake of the step, following the theory [16].

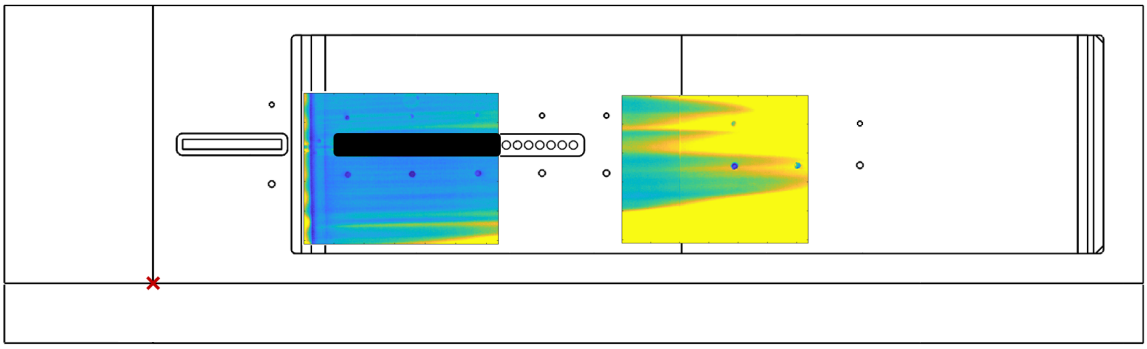

Fig 4. Top down view of the model showing IR results from two tests. Flow is from left to right.

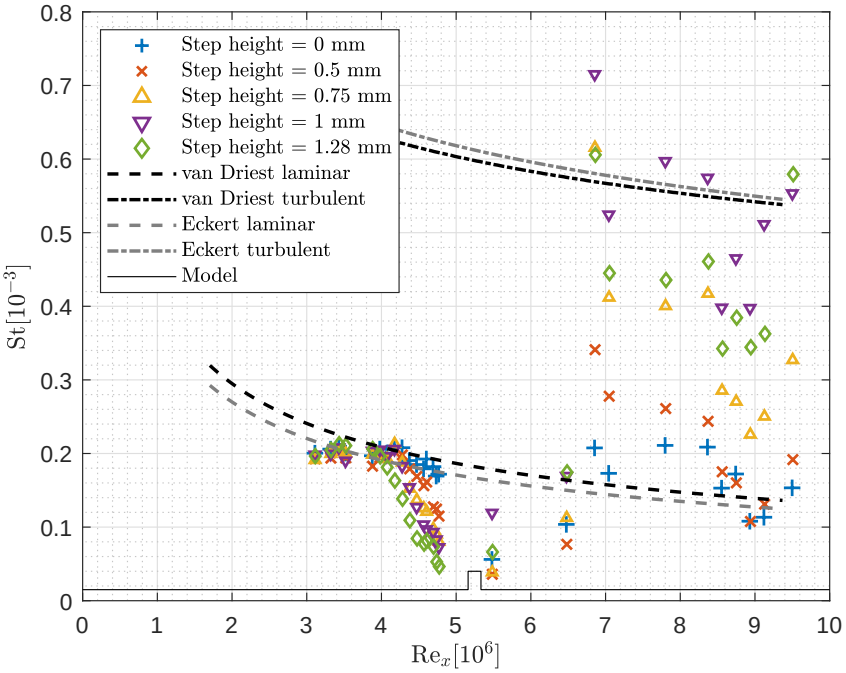

(a) Steps

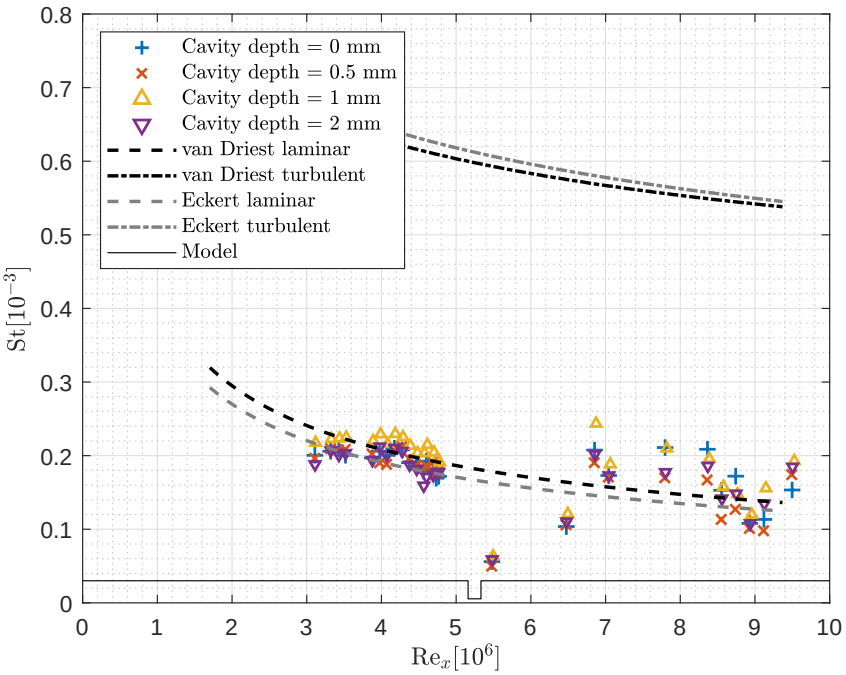

(b) Cavities

Fig 5. Stanton number vs Reynolds number plots for all the geometries tested, compared to laminar and turbulent flat plate correlations. The location of the step/cavity is shown at the bottom of each plot.

4.2. Surface Pressure

Surface pressure fluctuations were captured using PCB132 pressure transducers. Fig. 6 shows the summary of the pressure fluctuation data which is displayed as the power spectral density (PSD) of the surface pressure normalised by the freestream static pressure. PSDs were calculated using Welch's method [17] which efficiently provides an estimate of the frequency content of the signal.

Each plot shows the spectra for a single test at a single step height or cavity depth. The gauges are numbered 1 to 8, in increasing distance from the leading edge. Gauge 1 is upstream of the step and gauges 2 to 7 are all downstream. Positions of PCB sensors can be seen in Fig. 3, marked in red.

These plots show the frequency composition of pressure fluctuations in the boundary layer and serve two purposes: they can give an indication of what disturbance may be present and if there is a specific disturbance causing transition; and they can show whether or not the boundary layer is laminar or turbulent.

For the flat plate and steps (Fig. 6a to Fig. 6d), there is always some evidence of turbulent growth towards the rear of the plate, with the last gauge/s showing more energetic fluctuations than the upstream gauges (which are assumed to be laminar). This turbulent growth generally appears as a broadband increase, suggesting that there is no particular disturbance/frequency which ultimately leads to turbulence. The trend for larger steps is that the location of full turbulence moves upstream, although the 0.50 mm step appears to have little effect. In the two larger steps there appears to be a coherent peak at around 110 kHz upstream of the step, suggesting a particular flow feature is forming upstream of the step.

As with heat flux, cavities have a much smaller influence on pressure fluctuations. In Fig. 6e and Fig. 6f there is even an apparent stabilising effect with cavities, where gauges 7 and 8 sit at a lower level compared to the flat plate. It is unclear why this is the case. Only data for the 0.50 mm and the 2.00 mm cavities are shown as some of the gauges in the 1.00 mm test experienced large non-flow disturbances which highly affected the PSDs.

5. Conclusions

A sophisticated experimental model has been produced which is capable of high-precision in-situ adjustment of test geometries, employing a range of measurement techniques. The model now provides a platform for future experiments focusing on the effect of more representative surface geometries by combining more well understood, simple geometries. An initial dataset has been collected, showing some expected results and validating the choice of instrumentation. Additionally, some unexpected results have presented opportunity for further investigation: the scale of the decrease in heat flux upstream of steps was larger than expected and the effect of cavities on downstream boundary layer stability has been noted. In future work, model capability will also be extended: the implementation of interchangeable leading edges; possible axial relocation and resizing of the test geometry; and additional instrumentation to provide more insight into possible transition mechanisms.

6. Acknowledgements

This work was a de-risk activity funded by the European Space Agency under contract no. 4000129548. Thanks to the technical staff and tunnel operators at the Oxford Thermofluids Institute for consistent support during the experimental work.

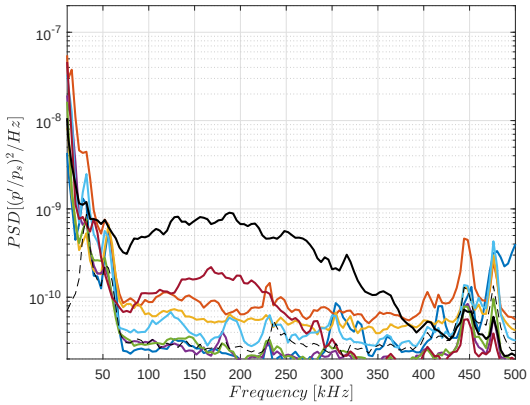

(a) Flat plate

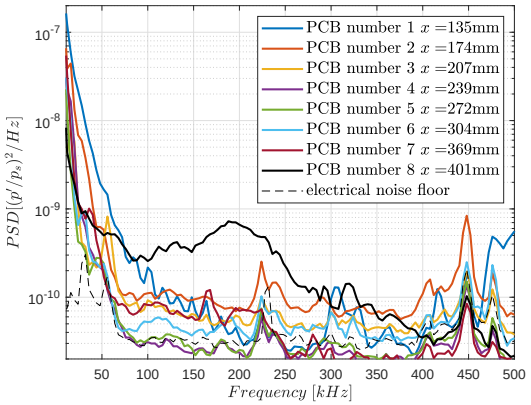

(b) 0.5 mm step

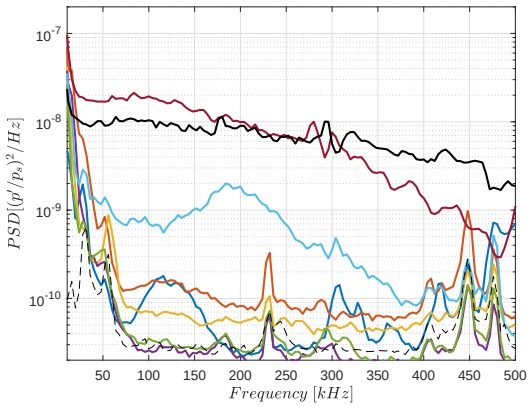

(c) 1.0 mm step

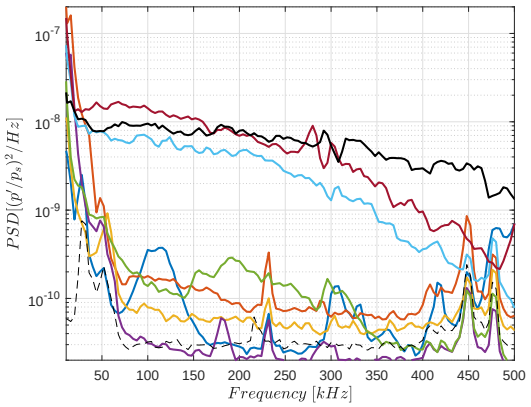

(d) 1.3 mm step

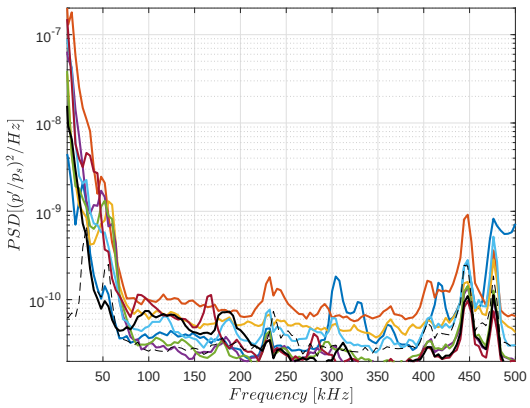

(e) 0.5 mm cavity

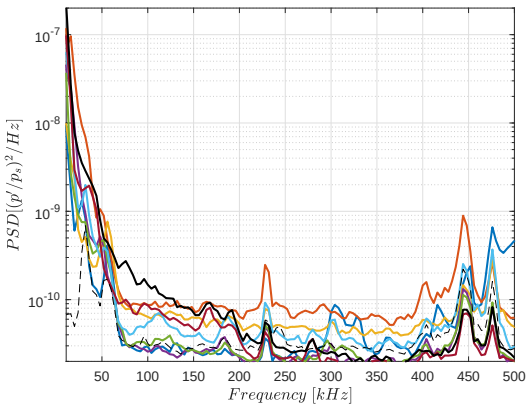

(f) 2 mm cavity

Fig 6. Power spectra of surface pressure fluctuations for different geometries.

References

[1] Steelant, J., Dalenbring, M., Kuhn, M., Bouchez, M., von Wolfersdorf, J.: Achievements obtained within ATLLAS-II on aero-thermal loaded material investigations for high-speed vehicles. 21st AIAA International Space Planes and Hypersonics Technologies Conference, p. 2393 (2017)

[2] Steelant, J., Varvill, R., Walton, C., Defoort, S., Hannemann, K., Marini, M.: Achievements obtained for sustained hypersonic flight within the LAPCAT-II project. 20th AIAA international space planes and hypersonic systems and technologies conference, p. 3677 (2015)

[3] Campbell, C., Anderson, B., Bourland, G., Bouslog, S., Cassady, A., Horvath, T., Berry, S., Gnoffo, P., Wood, W., Reuther, J., et al.: Orbiter return to flight entry aeroheating. 9th AIAA/ASME Joint Thermophysics and Heat Transfer Conference, p. 2917 (2006)

[4] McGilvray, M., Doherty, L.J., Neely, A.J., Pearce, R., Ireland, P.: The Oxford High Density Tunnel. 20th AIAA international space planes and hypersonic systems and technologies conference, p. 3548 (2015)

[5] Wylie, S., Doherty, L., McGilvray, M.: Commissioning of the Oxford high density tunnel (HDT) for boundary layer instability measurements at Mach 7. 2018 Fluid Dynamics Conference, p. 3074 (2018)

[6] Hillyer, J., Doherty, L., Hambidge, C., McGilvray, M.: Extension of test time in Ludwieg Tunnels. Second international conference on flight vehicles, aerothermodynamics and re-entry missions and engineering, Heilbronn, Germany (2022)

[7] Keyes, F.G.: The Heat Conductivity, Viscosity, Specific Heat and Prandtl Numbers for Thirteen Gases. Tech. rep., MASSACHUSETTS INST OF TECH CAMBRIDGE (1952)

[8] Petley, D., Smith, D., Edwards, C., Carlson, A., Hamilton, H.: Surface Step Induced Gap Heating in the Shuttle Thermal Protection System. Journal of Spacecraft and Rockets, 21(2):156–161 (1984)

[9] Collins, M., Chana, K., Povey, T.: New technique for the fabrication of miniature thin film heat flux gauges. Measurement science and technology, 26(2):025303 (2015)

[10] Hermann, T., McGilvray, M., Hambidge, C., Doherty, L., Buttsworth, D.: Total Temperature Measurements in the Oxford High Density Tunnel. International conference on flight vehicles, aerothermodynamics and re-entry missions and engineering, FAR, Monopoli, Italy (2019)

[11] Oldfield, M.: Impulse Response Processing of Transient Heat Transfer Gauge Signals. Journal of Turbomachinery (2008)

[12] Van Driest, E.R.: The Problem of Aerodynamic Heating. Institute of the Aeronautical Sciences (1956)

[13] Eckert, E.: Engineering Relations for Heat Transfer and Friction in High-Velocity Laminar and Turbulent Boundary-Layer Flow over Surfaces with Constant Pressure and Temperature. Transactions of the American Society of Mechanical Engineers, 78(6):1273–1283 (1956)

[14] Zakkay, V., Wang, C.R.: Applications of active cooling to nose cones. Tech. rep., NEW YORK UNIV BRONX SCHOOL OF ENGINEERING AND SCIENCE (1973)

[15] Grotowsky, I., Ballmann, J.: Numerical investigation of hypersonic step-flows. Shock Waves, 10(1):57–72 (2000)

[16] Nestler, D.: The Effects of Surface Discontinuities on Convective Heat Transfer in Hypersonic Flow. 20th Thermophysics Conference, p. 971 (1985)

[17] Welch, P.: The use of fast Fourier transform for the estimation of power spectra: a method based on time averaging over short, modified periodograms. IEEE Transactions on audio and electroacoustics, 15(2):70–73 (1967)